Concerted Emission and Local Potentiometry of Light-Emitting Electrochemical Cells

Deanna B. Rodovsky, Obadiah G. Reid, Liam S. C. Pingree, and David S. Ginger*

Department of Chemistry, University of Washington, Box 351700, Seattle, Washington 98195-1700

ARTICLE

ABSTRACT We study the operation of polymer light-emitting electrochemical cells (LECs) by combining scanning Kelvin probe microscopy with *in situ* imaging of the electroluminescence and photoluminescence on planar LECs. By combining these techniques on the same device in the same apparatus we directly map the relationship between the spatial distribution of electroluminescence and the local potential profile across the device. We find that the electroluminescence is always associated with a region of potential drop in LECs made with poly[2-methoxy-5-(3′,7′-dimethyl-octyloxy)-*p*-phenylenevinylene] (MDMO-PPV), poly(ethylene oxide)(PEO), and potassium trifluoromethanesulfonate. Nevertheless, depending on the electrode metal used, we also find significant potential drops at or near the electrode/organic interfaces. We study the effects of using different electrodes and show that both the electroluminescence and potential profiles are strongly dependent on the electrode work function for thin junctions operated at low potentials. These results indicate injection barriers can affect the operation of LECs even in the presence of doping.

KEYWORDS: light-emitting electrochemical cells (LECs) · planar · electroluminescence · photoluminescence · atomic force microscopy (AFM) · scanning Kelvin probe microscopy (SKPM) · organic electronic devices · electrogenerated chemiluminescence · operation mechanism · electrode · metal work function

Polymer light-emitting electrochemical cells (LECs) are solid-state devices comprising a blend of light-emitting polymer, solid state ion-transport agent, and salt.[1] They have received interest owing to their compatibility with solution-based fabrication processes, especially printable conductive electrodes.[2−4] However, the exact mechanism of LEC operation has remained controversial despite the improvements in efficiency, lifetime, and response rates that have occurred in recent years.[5−12] Broadly, the LEC operation models fall into three classes: (1) an ideal p-i-n junction model,[1] where symmetric n-type and p-type doping take place and both the majority of the potential drop and the electroluminescence occur in a central undoped (intrinsic) region of the device; (2) an electrodynamic model[13] in which the majority of the applied potential is dropped across ionic double-layers at the electrode/polymer interfaces; and (3) a preferential p-type doping model[14] in which the majority of the device is p-type doped and the potential drop and electroluminescence occurs much closer to the cathode than the anode. These models have been studied mainly by electroabsorption,[15,16] optical beam induced current,[17] and fluorescence microscopy.[5,9,18−30]

Recently, our group,[31] Slinker *et al.*,[32] and Matyba *et al.*,[30] have all used scanning Kelvin probe microscopy (SKPM) to directly measure the potential profiles across biased planar LECs. Nevertheless, even these three studies have produced results that appear contradictory. Slinker *et al.* found the largest potential drop adjacent to the cathode despite the maximum electroluminescence being observed adjacent to the anode. Consistent with the study of Slinker *et al.*, our group observed the largest potential drop adjacent to the cathode.[31] Most recently, Matyba *et al.* reported that both the electroluminescence peak and the largest potential drop occurred offset from the cathode by ~20% of the interelectrode gap.[30] The different results from these three papers may arise from the fact that all three groups used varied combinations of light-emitting materials and ionic salts and this is known to impact the position, shape, and intensity of the emission in optical experiments.[5,25] Unfortunately, the relationship between the electroluminescence and SKPM must be inferred indirectly from these experiments because both Slinker *et al.* and Matyba *et al.* performed the electroluminescence and SKPM imaging in separate experiments on different devices. Because the properties of LEC junctions are known to evolve in time,[19−21,28,33] the lack of spatially correlated electroluminescence and SKPM data prevents a meaningful

*Address correspondence to ginger@chem.washington.edu.

Received for review February 18, 2010 and accepted April 19, 2010.

Published online April 27, 2010.
10.1021/nn1003315

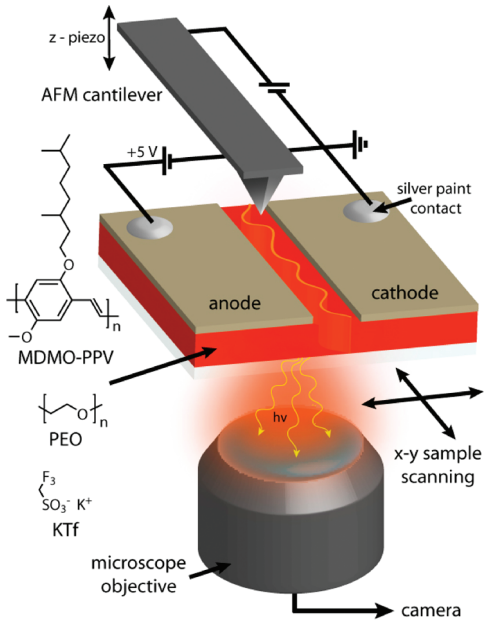

Figure 1. Schematic diagram of the experiment configuration in forward bias. The polymer layer is spin-coated prior to electrode deposition. The device is mounted to allow collection of optical and scanning Kelvin probe microscopy images on the same device. The atomic force microscope probe is raster-scanned across the interelectrode gap with the cantilever axis parallel to the long axis of the gap. Optical images of the photoluminescence and electroluminescence images are collected *via* an inverted microscope and camera.

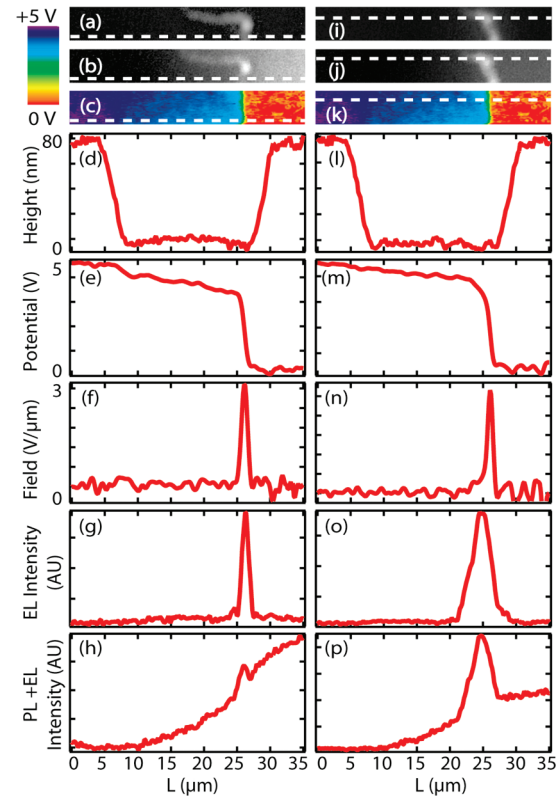

Figure 2. Electroluminescence (EL), photoluminescence (PL), and SKPM images of an Au/MDMO-PPV, PEO, KTf/Au planar LEC under +5 V bias (left electrode is the anode, right electrode is the cathode) showing good correlation between the electroluminescence maximum and potential drop in the device: (a) electroluminescence image at 2 min, (b) photoluminescence and electroluminescence image at 2 min, (c) SKPM image collected from 2 to 6 min (SKPM scan is initiated immediately following the capture of optical images), (d) height trace indicating electrode edges with respect to dashed lines in panels a−c, (e) 2 line-averaged potential profile from the bottom of panel c as indicated by the dashed line, (f) electric field profile obtained by numerical differentiation of the potential profile in panel e, (g) electroluminescence line profile from the region indicated by the dashed line in panel a, and (h) photoluminescence and electroluminescence line profile from the region indicated by the dashed line in panel b. After the SKPM image acquisition (c) is complete, optical images are collected: (i) electroluminescence image at 6 min, (j) photoluminescence and electroluminescence image at 6 min, (k) SKPM image collected from 2 to 6 min and the dashed line corresponds to the line trace panel m, (l) height trace indicating electrode edges with respect to dashed lines in panels i−k, (m) 2 line-averaged potential profile from the top of panel k as indicated by the dashed line, (n) electric field profile obtained by numerical differentiation of the potential profile in panel m, (o) electroluminescence line profile from the region indicated by the dashed line in panel i, and (p) photoluminescence and electroluminescence line profile from the region indicated by the dashed line in panel j.

comparison between the quantitative potential profiles that have been extracted using SKPM with the much wider body of literature that have inferred potential profiles based on optical imaging.

In this paper, we report studies of LECs in which both SKPM and high-resolution electroluminescence imaging can be directly correlated on the same device (Figure 1). We use these methods to study an archetypal LEC structure consisting of poly[2-methoxy-5-(3′,7′-dimethyl-octyloxy)-*p*-phenylenevinylene] (MDMO-PPV), poly(ethylene oxide) (PEO), and potassium trifluoromethanesulfonate (KTf). We study the device operation mechanism when varying the work function of the electrode. We observe that electroluminescence is always closely associated with a region of localized potential drop, but we demonstrate that the work function of the metal affects device operation in μm-gap LECs resulting in strikingly different electroluminescence and potential profiles with gold, aluminum, or calcium electrodes.

RESULTS AND DISCUSSION

We begin by examining planar LECs with gold electrodes as studied by a number of authors.[5,9,23−31,33] When using lithium trifluoromethanesulfonate (LiTf) as the salt, we observe electroluminescence adjacent to the cathode (see Supporting Information, Figure S1), which is consistent with our original SKPM report[31] as well as the work of Edman and co-workers.[23,25] In contrast, when we replace lithium with potassium (using KTf as the salt) we observe electroluminescence that is offset from the cathode by a small fraction of the interelectrode gap within minutes after the application of a +5 V bias (Figure 2a). This sensitivity of the electroluminescence position to the choice of counterion is consistent with the results of Edman and co-workers.[9,25,28]

We speculate that the difference in electroluminescence position may be related to ion mobility in the film, but is not a central focus of this paper. Since KTf allows us to observe electroluminescence within the interelectrode region, we used KTf for the devices in this study.

Figure 2 panels b and c show the corresponding photoluminescence and SKPM images captured immediately after the electroluminescence in Figure 2a. We observe a decrease in photoluminescence (Figure 2b,h) propagating from both electrodes consistent with the observations of other groups characterizing similar devices.[5,9,28] Figure 2g shows the electroluminescence, which reaches a maximum within the interelectrode gap, yet is much closer to the cathode than the anode. We correlate these optical images with our SKPM data through graphical comparison of features visible in both the optical and AFM topography images (see Experimental Section). The dashed line on the SKPM image (Figure 2c) corresponds to the SKPM line trace shown in Figure 2e, which is acquired within the first minute of scanning (SKPM scan is collected from bottom to top of the image). By performing these measurements *in a concerted manner on the same device*, we are able to establish that the maximum potential drop and highest field (Figure 2e,f) correlate with the position of maximum electroluminescence (Figure 2g). Since the electroluminescence in our gold-electrode LECs moves with time (roughly 0.5−2 μm/min) as has been reported by others,[29] we also rule out movement on the time-scale of our experiments by performing optical imaging both pre- and post-SKPM imaging (Figure 2 panels a,b and i,j, respectively). We correlate the regions of the post-SKPM optical images (as indicated by the dashed lines in Figure 2i,j) to traces collected at the end of the SKPM scan (as indicated by the dashed line in Figure 2k). Although the electroluminescence moves closer to the cathode as a function of time (Figure 2i), the electroluminescence maximum and potential drop are still well-correlated (Figure 2m,o), demonstrating that the evolution is slow enough for us to extract the relationship between the optical and potential profiles for gold-electrode LECs.

After capturing the post-SKPM optical images we confirm the reversible operation of our devices by inverting the bias and driving the same device at −5 V (see Supporting Information, Figure S2). After approximately one minute we observe faint emission on the opposite side of the device, and the SKPM and electroluminescence profiles collected at −5 V are mirror images of those collected at +5 V as shown in Figure 2. Our results demonstrate the stability/reversibility of the junctions under these conditions and time scales, as expected for dynamic-junction LECs with freely mobile counterion distributions.[34]

These results lead us to two significant conclusions. First, because our SKPM and optical imaging are performed in the same optical microscope, we are able to establish exact registry between our potential profiles and electroluminescence images (see Experimental Section for additional details). Therefore, we can conclude that the electroluminescence and potential drop maximum occur at the same point in the device for PPV-based LECs. Although such a correlation has been assumed by many authors, it has never been directly correlated for any type of LEC. Establishing this correlation given the materials used is important, since separate electroluminescence and SKPM data collected using a different light-emitting complex (ruthenium trisbipyridine hexafluorophosphate or $[Ru(bpy)_3]^{2+}(PF_6^-)_2$) have suggested that the maximum electroluminescence and maximum potential drop may be uncorrelated in LECs made with $[Ru(bpy)_3]^{2+}(PF_6^-)_2$.[32]

In addition to providing a correlation between the electroluminescence and potential profiles, our data provide a test for the three models of LEC operation (ideal p-i-n junction,[1] electrodynamic,[13] and preferential p-type[14]) that have dominated the literature. For gold-electrode LECs we observe photoluminescence quenching in the device, and we observe that the electroluminescence is much closer to the cathode than to the anode (the latter in contrast to the ideal p-i-n model). Nevertheless, when using KTf as the salt, we observe that most of the electroluminescence and potential drop occur a finite distance from the cathode. Thus, while the data are not perfectly consistent with an ideal symmetric p-i-n structure, they do provide evidence of a large field drop away from the electrode as proposed by that model. However, the region associated with p-type doping is much larger than the region associated with n-type doping, as has been observed by many authors.[5,9,18−30] While our observations would thus seem to favor the preferential p-type doping model, we do observe limited n-type doping. Therefore, we suggest that the three proposed models[1,13,14] be viewed as extreme points along a continuum rather than mutually exclusive pictures: it is possible for devices to exhibit behavior consistent with all three depending on the fabrication and operating conditions.

Here, in addition to correlating and establishing the position of electroluminescence and potential drop maximum in the interelectrode region, we seek to better understand the observed variations in operation. We consider the possibility that even in the presence of electrochemical doping and potential side reactions[9] the choice of electrode and the corresponding charge injection barriers do affect LEC operation. Indeed, Gao and co-workers have reported data collected from 1 mm-gap PPV-based devices driven at high drive voltages (+250 V) that suggest such an effect is possible.[27] Further, Malliaras and co-workers report differences in brightness and efficiency in charged iridium complex LECs that can be attributed to electrode selection.[35] We thus turn to examine the possible role of metal work

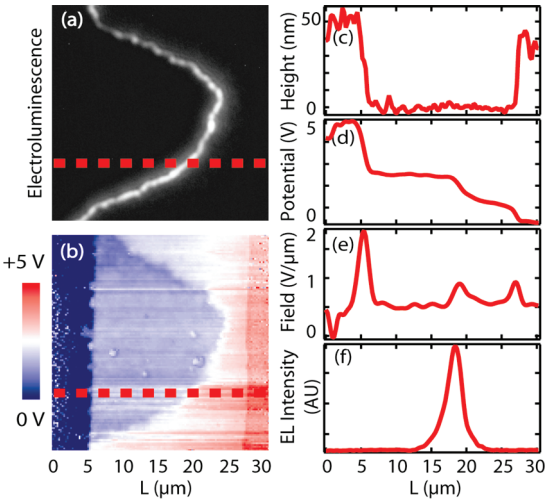

Figure 3. Electroluminescence (EL) and SKPM images of an Al/MDMO-PPV, PEO, KTf/Al planar LEC under +5 V bias (left electrode is the anode, right electrode is the cathode) showing potential drops at both the anode and cathode as well as in the interelectrode region of the device. The interelectrode potential drop correlates to the region of maximum electroluminescence: (a) electroluminescence image captured at 10 min, (b) SKPM image acquired from 11 to 30 min, (c) height trace from SKPM image b indicating electrode edges, (d) 4 line-averaged potential profile from image b as indicated by the dashed line, (e) electric field profile obtained by numerical differentiation of the voltage profile d, and (f) electroluminescence line profile from the region indicated by the dashed line in image a.

function on the operation of an LEC by comparing the properties of LECs with aluminum and calcium electrodes to those with gold electrodes.

Figure 3 shows the electroluminescence from a planar LEC identical to that shown in Figure 2, except made with aluminum electrodes. In contrast to the gold device, the electroluminescence observed with aluminum electrodes is much wavier, but spans the entire interelectrode region (rather than being close to the cathode as we always observe in gold devices). In our smaller-gap (μm-size) devices operated at +5 V bias, we also observe much slower movement of the electroluminescence region with aluminum-electrode *versus* gold-electrode devices (~100 to 200 nm/min *vs* ~0.5 to 2 μm/min). As a result, the aluminum-electrode devices exhibit a more stable junction and longer lifetime (>1 h) in our studies. The relative stability of the aluminum-electrode devices allows us to capture larger SKPM images as shown in Figure 3b. We note that the SKPM image is again well-correlated to the electroluminescence image (Figure 3a). The line trace in Figure 3d is extracted from the region indicated by the dashed line in the SKPM image (Figure 3b). We observe potential drops at both the anode and cathode as well as in the interelectrode region of the device. Figure 3f shows the electroluminescence profile along the same line section, which correlates with the region of potential drop in the interelectrode region in Figure 3d. Even though the SKPM and optical profiles evolve more slowly in time for aluminum electrodes than with gold electrodes, we collect post-SKPM optical images for comparison. Optical and post-SKPM images are also well-correlated at different times and regions in the device, confirming that any motion of the junction during imaging has a negligible affect on our conclusions. We also observe an increase in photoluminescence quenching in the interelectrode region as a function of time (see Supporting Information, Figure S3).

A comparison of Figures 2 and 3 shows that both the electroluminescence and potential profiles are significantly different between planar LECs made with gold and aluminum electrodes. We hypothesize that these differences result from the position of the electrode work function relative to the highest occupied molecular orbital (HOMO) and lowest unoccupied molecular orbital (LUMO) of MDMO-PPV. When using MDMO-PPV with gold-electrode LECs, hole injection into the HOMO should be facile due to the close proximity of the metal Fermi level to the HOMO of the polymer. In contrast, the work function of aluminum is lower than gold and nearly centered between the HOMO and LUMO of MDMO-PPV, which could lead to more balanced hole and electron injection and centrally located junctions. The potential drops we observe at the aluminum/polymer interface could thus reflect the field needed to overcome an injection barrier at the metal/polymer interface. While the build up of a highly charged layer at metal/organic interface can be accounted for in both the p-i-n junction and electrodynamic models, the strong variation in barrier heights shows that the nature of the contact can have a clear influence on the internal potential profile and the operating mechanism of an LEC. We conclude that LECs may be able to operate in a regime involving some aspects of both the p-i-n junction and electrodynamic models depending on the device structure.

To further test our hypothesis that the position of the metal Fermi level with respect to the polymer HOMO and LUMO levels can affect the operating mechanism of an LEC, we also examine planar devices using calcium electrodes. Figure 4 panels a, b, and c show photoluminescence, electroluminescence, and SKPM for a set of planar LECs with calcium electrodes driven at +5, +40, and +5 V, respectively. We observe only slight photoluminescence quenching in the interelectrode region (Figure 4a). No electroluminescence is observed during the testing period of approximately 30 min of driving at +5 V. Noting there may be a larger barrier to charge injection that could be overcome by increasing the applied bias, we increase the bias in increments of +10 up to +40 V at which point we observe electroluminescence adjacent to the anode (Figure 4b). On a similar device to those shown in Figure 4a,b, we collect an SKPM image of a device driven at +5 V (Figure 4c). From the SKPM line trace (Figure 4c), we calculate that ~90% of the potential drop occurs adja-

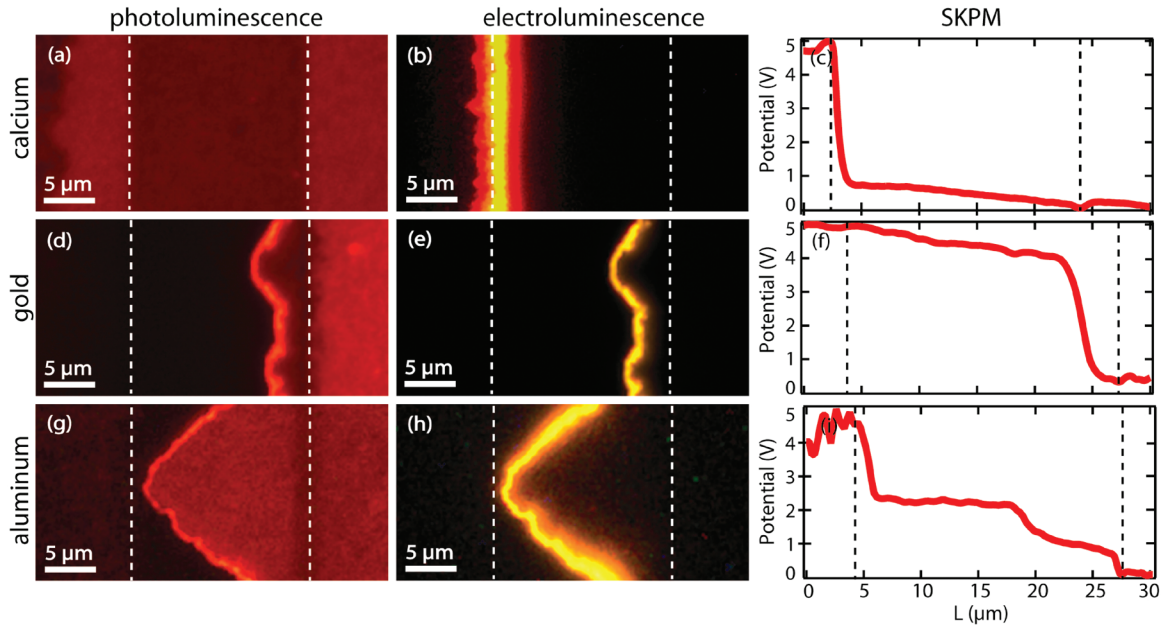

Figure 4. A comparison of calcium-, gold-, and aluminum-electrode LECs demonstrating the striking differences in the photoluminescence, electroluminescence, and potential profiles when the electrode selection is varied: (a) photoluminescence of a calcium-electrode LEC driven at +5 V, (b) electroluminescence of image a driven at +40 V, (c) SKPM potential profile of a calcium LEC operated at +5 V, (d) photoluminescence of a gold-electrode LEC driven at +5 V, (e) electroluminescence of image d, (f) SKPM potential profile of a gold-electrode LEC driven at +5 V, (g) photoluminescence of an aluminum-electrode LEC driven at +5 V, (h) electroluminescence of image g, (i) SKPM potential profile of an aluminum-electrode LEC operated at +5 V. In all images, the left electrode is the anode and the right electrode is the cathode. Dashed lines indicate the electrode edge.

cent to the anode within our resolution. We note that the photoluminescence, electroluminescence, and SKPM images are taken under different drive conditions, since we are unable to obtain electroluminescence from calcium-electrode devices under biases compatible with simultaneous SKPM imaging. Nevertheless, the images in Figure 4a−c are consistent both with the correlations established for gold- and aluminum-electrode devices and with the hypothesis that the electrode work function impacts device performance.

To facilitate comparison of the device profiles as a function of electrode type, Figure 4 panels d−i show representative photoluminescence, electroluminescence, and SKPM images of gold- and aluminum-electrode devices alongside the calcium-electrode devices. Because of the well-matched HOMO of the polymer (5.3 eV)[36] and the work function of gold (Φ = 5.31 to 5.47 eV),[37] hole injection will be favored over electron injection when a positive bias is applied to a gold-electrode LEC. Indeed, we observe a spatially more dominant p-type than n-type region in such devices as shown by a more uniform electroluminescence and potential drop closer to the cathode (Figure 4g−i). When we change to aluminum electrodes (Φ = 4.06−4.26 eV),[37] we note the work function of aluminum is nearly centered between the HOMO and LUMO (3.0 eV)[36] of the polymer. Here, we typically observe a wavy line of electroluminescence spanning the interelectrode region consistent with more balanced hole and electron injection. With a low-work function metal such as calcium (Φ = 2.87 eV),[37] electron injection from the cathode into the polymer LUMO is favored. Consistent with our hypothesis, the calcium-electrode devices exhibit the largest potential drop at the anode suggesting that for these devices electrons are more readily injected into the active layer than holes. Under these circumstances, electrons migrate toward the anode, and charge recombination occurs very near the metal/polymer interface at the opposite electrode (anode). The observed sensitivity of the position of electroluminescence to the work function of the electrode metal in our experiment contrasts with literature results on mm-gap devices driven at higher voltages (+250 V).[27] However, we note that such high voltages can provide ample potential to overcome likely injection barriers of only a few eV, and thus may be more sensitive to transport rather than injection effects. Given that practical vertical devices are typically ~1 μm or less in thickness and driven with only a few volts, we believe our results collected on μm-gap devices at lower biases may better reflect the operation of vertical device structures that are of ultimate interest for applications.

CONCLUSIONS

These concerted SKPM and optical microscopy experiments enable us to directly correlate the local potential and electroluminescence profiles in μm-gap planar LECs operated under low voltage conditions relevant to vertical LECs. Our results show well-correlated electroluminescence and potential profiles

in LECs using an alkoxy-PPV as the emitter, thus enabling the analysis of a wide body of literature on optical imaging of similar systems. With regard to the controversy surrounding the mechanism of LEC operation, our results show that devices can exhibit characteristics of all three prevailing models at the same time, including a correlated region of electroluminescence and potential drop in the interelectrode gap consistent with the p-i-n model,[1] uncompensated charge and fields at the metal/polymer interfaces consistent with the electrodynamic model,[13] and a preference for either p- or n-type doping consistent with the preferential p-type model.[14] By varying the work function of the electrode metal, we are able to change both the relative potential profile and the corresponding electroluminescence profile indicating that even if an LEC emits light at a low voltage, the underlying operation mechanism can still be sensitive to the presence of injection barriers at the electrodes. Not only do these results suggest new directions that could be used to improve the performance and viability of future LECs (for example, tailoring polymer energy level or surface functionalization of printed electrodes to optimize the metal/organic contacts), but also, given the role that ions can play in a wide range of applications[38] (chemical sensors, electrochemical transistors, and photoelectrochemical cells), these tools and our improved understanding of the operation of these model solid-state electrochemical devices should have impacts beyond the field of organic LECs.

EXPERIMENTAL SECTION

Materials. The materials used in this study include lithium trifluoromethanesulfonate (lithium triflate or LiTf, 99.995%, Aldrich), potassium trifluoromethanesulfonate (potassium triflate or KTf, 99%, Acros), poly(ethylene oxide) (PEO, M_w = 900 000 g mol^{-1}, Acros), and poly[2-methoxy-5-(3′,7′-dimethyl-octyloxy)-*p*-phenylenevinylene] (MDMO-PPV). PEO was used as received. KTf was dried at a temperature of 100 °C under vacuum prior to use. The light-emitting polymer, MDMO-PPV, was synthesized in-house using a Gilch polymerization route *via* dehydrohalogenation of appropriate precursors as outlined in the literature.[39] The average molecular weight was approximately 530 000 and the polydispersity index (PDI) was 1.03.

Device Fabrication. All device fabrication, with the exception of substrate cleaning, was performed in a nitrogen glovebox (<1 ppm O_2) with an integrated evaporation chamber. The glass substrates (1 × 1 cm^2) were cleaned by successive ultrasonic treatment in a diluted soap solution (1% Micron-90 in deionized water), water, acetone, and isopropanol for 30 min in each bath. The substrates were then plasma cleaned for 10 min and immediately loaded into the glovebox. A bulk solution was prepared by dissolving 25 mg of PEO and 9 mg of KTf in 20 mL of cyclohexanone (≥99.0%, ≤ 0.05% water, Aldrich). The polymer blend solution was prepared by mixing the bulk solution with 8 mg of MDMO-PPV in a mass ratio of MDMO-PPV/PEO/KTf = 1.0:0.375:0.125 followed by stirring on a magnetic hot plate at 65 °C for 24 h. The polymer films were spin-coated to a thickness of 250−350 nm (as determined by AFM measurements). After spin-coating, the polymer films were annealed on a hot plate at 90 °C for 1 h in the glovebox. The interelectrode gap was defined by pulling a gold wire (~20 μm, Thermionic Products) taut over and perpendicular to the long edge of the mask area (0.1 mm × 15 mm), securing the wire onto the electrode mask, and subsequently fixing the substrate to the mask in conformal contact. The films were loaded into the thermal evaporator and dried under vacuum at 10^{-7} Torr overnight. A top contact was evaporated onto the substrate by thermal evaporation (~50 nm, 1 Å/s, $P \approx 5 \times 10^{-7}$ Torr). Samples were then loaded into a closed fluid cell (Asylum Research) fitted with the appropriate tubing and valves to ensure no ambient exposure on removal from the glovebox. As the closed fluid cell was removed from the glovebox, it was immediately placed on a cart, purged with high-purity N_2, transferred to the atomic force microscope (AFM), and left under a constant flow of gas for the remainder of the experiment. The cart consists of a small-format high-purity N_2 cylinder, a gas purification trap (Aldrich), a flow meter (McMaster), precleaned copper tubing (McMaster), PTFE tubing (McMaster), and miniature ball valves (McMaster).

Optical and Scanning Probe Microscopy. SKPM measurements were performed using an Asylum Research MFP-3D AFM, a Stanford Research Systems model 830 lock-in amplifier, an Agilent Technologies 33120A function generator, and a custom-built summing amplifier. Cr/Pt coated silicon AFM probes (BudgetSensors, Tap300E, spring constant = 40 N/m, 300 kHz resonance) were chosen for these experiments. The AFM was mounted on an inverted optical microscope (Nikon TE2000-U) to enable optical imaging of the area scanned using the AFM. The sample was illuminated either through the built-in optics of the MFP-3D (above the cantilever; used for rough positioning of the tip relative to the active area of the device) or using the inverted optical microscope (photoluminescence excitation). Biases were applied across the two electrodes at +5 VDC, except as noted otherwise (calcium-electrode devices). The cantilever was oriented parallel to the long axis of the gap to minimize artifacts due to the capacitance between the cantilever beam and the electrodes.[40] Scanning was performed in the direction perpendicular to the long axis of the gap as indicated in Figure 1.

All SKPM images (surface potential) were acquired in a two-pass (line-by-line), phase-detection implementation. During the first pass the topography was acquired through a regular tapping-mode scan. In the second, the tip is lifted a constant height above the recorded surface topography and rescanned to obtain the surface potential. Surface potential measurements were made by applying an alternating current (AC) bias that is spectrally distant from any mechanical resonance of the cantilever and much lower than the primary resonance (700 Hz, 2 V peak-to-peak). The phase-response of the primary cantilever resonance at the applied AC frequency (700 Hz) is then nulled by applying a DC bias to the cantilever, thereby providing a measurement of the contact-potential difference between the tip and sample surface.

A lift height of 30−50 nm was used for all SKPM measurements with a tip dwell time of 10 ms per pixel during SKPM image acquisition and a tip velocity of 10 μm/sec during the topography scan. These values were chosen as an appropriate compromise between imaging stability, lateral resolution, and image acquisition time (typical scan acquisition time varied from ~5 min to ~20 min depending on the sample). Optical images of the electroluminescence and photoluminescence were obtained using an inverted microscope (Nikon TE2000-U) and collected *via* an integrated camera (Pixera Penguin 150 CLM or Diagnostic Instruments Spot Flex). For photoluminescence images, a 505 nm light-emitting diode (Luxeon) or halogen lamp (Nikon) was used as the excitation source. The excitation and emission light were separated with bandpass (470 nm/40 nm), dichroic (500 nm), and long-pass (610 nm/40 nm) filters. We aligned our optical microscopy and AFM images by collecting optical (transmission) and AFM topography images on a featured region of the sample. The Cartesian coordinate transform (angle, scale, and translation) that maps the AFM measurements onto the optical images is obtained by graphical comparison of the size and orientation of the randomly distributed surface features in the optical and AFM images.

Acknowledgment. This paper is based on work supported by the NSF (DMR-0120967 & DMR-0449422) as well as the DOE and AFOSR. D. Ginger thanks the Camille Dreyfus Teacher-Scholar Awards Program for support, the Cottrell Scholar of the Research Corporation, and the Alfred P. Sloan Foundation for support during the period of this work. L. Pingree acknowledges the support of the NSF Discovery Corps Fellowship Program (CHE0725139) and O. Reid acknowledges that this research was supported in part by the Center for Nanotechnology at the University of Washington through an Integrative Graduate Education and Research Traineeship (IGERT) Fellowship Award NSF (DGE-0504573).

Supporting Information Available: Electroluminescence of a LiTf-based LEC using the same device fabrication methods as the KTf-based device in Figure 2. Electroluminescence, photoluminescence, and SKPM images of an Au/MDMO-PPV, PEO, KTf/Au planar LEC driven at −5 V after first driving at +5 V (Figure 2). Electroluminescence, photoluminescence, and SKPM images of an Al/MDMO-PPV, PEO, KTf/Al planar LEC driven at +5 V (the same device as shown in Figure 3). This material is available free of charge *via* the Internet at http://pubs.acs.org.

REFERENCES AND NOTES

1. Pei, Q. B.; Yu, G.; Zhang, C.; Yang, Y.; Heeger, A. J. Polymer Light-Emitting Electrochemical Cells. *Science* **1995**, *269*, 1086–1088.
2. Skotheim, T. A.; Reynolds, J. R., *Handbook of Conducting Polymers*, 3rd ed.; CRC Press: Boca Raton, 2007; Vol. II.
3. Lee, H. H.; Chou, K. S.; Huang, K. C. Inkjet Printing of Nanosized Silver Colloids. *Nanotechnology* **2005**, *16*, 2436–2441.
4. Gamerith, S.; Klug, A.; Scheiber, H.; Scherf, U.; Moderegger, E.; List, E. J. W. Direct Ink-Jet Printing of Ag−Cu Nanoparticle and Ag-Precursor Based Electrodes for OFET Applications. *Adv. Funct. Mater.* **2007**, *17*, 3111–3118.
5. Matyba, P.; Andersson, M. R.; Edman, L. On the Desired Properties of a Conjugated Polymer-Electrolyte Blend in a Light-Emitting Electrochemical Cell. *Org. Electron.* **2008**, *9*, 699–710.
6. Shao, Y.; Bazan, G. C.; Heeger, A. J. Long-Lifetime Polymer Light-Emitting Electrochemical Cells. *Adv. Mater.* **2007**, *19*, 365–370.
7. Leger, J. M.; Rodovsky, D. B.; Bartholomew, G. R. Self-Assembled, Chemically Fixed Homojunctions in Semiconducting Polymers. *Adv. Mater.* **2006**, *18*, 3130–3134.
8. Shao, Y.; Gong, X.; Heeger, A. J.; Liu, M.; Jen, A. K. Y. Long-Lifetime Polymer Light-Emitting Electrochemical Cells Fabricated with Crosslinked Hole-Transport Layers. *Adv. Mater.* **2009**, *21*, 1972–1975.
9. Fang, J.; Matyba, P.; Robinson, N. D.; Edman, L. Identifying and Alleviating Electrochemical Side-Reactions in Light-Emitting Electrochemical Cells. *J. Am. Chem. Soc.* **2008**, *130*, 4562–4568.
10. Zhang, Y. G.; Gao, J. Lifetime Study of Polymer Light-Emitting Electrochemical Cells. *J. Appl. Phys.* **2006**, *100*, 084501-1–084501-8.
11. Zhang, Y. G.; Hu, Y. F.; Gao, J. Improving the Efficiency of Polymer Light-Emitting Electrochemical Cells by Controlled Doping Relaxation. *Appl. Phys. Lett.* **2006**, *88*, 163507-1–163507-3.
12. Bolink, H. J.; Coronado, E.; Costa, R. D.; Orti, E.; Sessolo, M.; Graber, S.; Doyle, K.; Neuburger, M.; Housecroft, C. E.; Constable, E. C. Long-Living Light-Emitting Electrochemical Cells—Control Through Supramolecular Interactions. *Adv. Mater.* **2008**, *20*, 3910–3913.
13. deMello, J. C.; Tessler, N.; Graham, S. C.; Friend, R. H. Ionic Space-Charge Effects in Polymer Light-Emitting Diodes. *Phys. Rev. B* **1998**, *57*, 12951–12963.
14. Leger, J. M.; Carter, S. A.; Ruhstaller, B. Recombination Profiles in Poly[2-methoxy-5-(2-ethylhexyloxy)-1,4-phenylenevinylene] Light-Emitting Electrochemical Cells. *J. Appl. Phys.* **2005**, *98*, 124907-1–124907-7.
15. deMello, J. C.; Halls, J. J. M.; Graham, S. C.; Tessler, N.; Friend, R. H. Electric Field Distribution in Polymer Light-Emitting Electrochemical Cells. *Phys. Rev. Lett.* **2000**, *85*, 421–424.
16. Gao, J.; Heeger, A. J.; Campbell, I. H.; Smith, D. L. Direct Observation of Junction Formation in Polymer Light-Emitting Electrochemical Cells. *Phys. Rev. B* **1999**, *59*, R2482–R2485.
17. Dick, D. J.; Heeger, A. J.; Yang, Y.; Pei, Q. B. Imaging the Structure of the p-n Junction in Polymer Light-Emitting Electrochemical Cells. *Adv. Mater.* **1996**, *8*, 985–987.
18. Gao, J.; Dane, J. Planar Polymer Light-Emitting Electrochemical Cells with Extremely Large Interelectrode Spacing. *Appl. Phys. Lett.* **2003**, *83*, 3027–3029.
19. Hu, Y. F.; Tracy, C.; Gao, J. High-Resolution Imaging of Electrochemical Doping and Dedoping Processes in Luminescent Conjugated Polymers. *Appl. Phys. Lett.* **2006**, *88*, 123507-1–123507-4.
20. Gao, J.; Dane, J. Visualization of Electrochemical Doping and Light-Emitting Junction Formation in Conjugated Polymer Films. *Appl. Phys. Lett.* **2004**, *84*, 2778–2780.
21. Gao, J.; Dane, J. Imaging the Doping and Electroluminescence in Extremely Large Planar Polymer Light-Emitting Electrochemical Cells. *J. Appl. Phys.* **2005**, *98*, 063513-1–063513-8.
22. Hu, Y. F.; Zhang, Y. G.; Gao, J. Strong Electroluminescence from Polymer Films with Heavily Quenched Photoluminescence. *Adv. Mater.* **2006**, *18*, 2880–2883.
23. Shin, J. H.; Dzwilewski, A.; Iwasiewicz, A.; Xiao, S.; Fransson, A.; Ankah, G. N.; Edman, L. Light Emission at 5 V from a Polymer Device with a Millimeter-Sized Interelectrode Gap. *Appl. Phys. Lett.* **2006**, *89*, 013509-1–013509-3.
24. Shin, J. H.; Xiao, S.; Edman, L. Polymer Light-Emitting Electrochemical Cells: The Formation and Effects of Doping-Induced Micro Shorts. *Adv. Funct. Mater.* **2006**, *16*, 949–956.
25. Shin, J. H.; Robinson, N. D.; Xiao, S.; Edman, L. Polymer Light-Emitting Electrochemical Cells: Doping Concentration, Emission-Zone Position, and Turn-On Time. *Adv. Funct. Mater.* **2007**, *17*, 1807–1813.
26. Shin, J. H.; Matyba, P.; Robinson, N. D.; Edman, L. The Influence of Electrodes on the Performance of Light-Emitting Electrochemical Cells. *Electrochim. Acta* **2007**, *52*, 6456–6462.
27. Hohertz, D.; Gao, J. How Electrode Work Function Affects Doping and Electroluminescence of Polymer Light-Emitting Electrochemical Cells. *Adv. Mater.* **2008**, *20*, 3298–3302.
28. Robinson, N. D.; Fang, J. F.; Matyba, P.; Edman, L. Electrochemical Doping During Light Emission in Polymer Light-Emitting Electrochemical Cells. *Phys. Rev. B* **2008**, *78*, 245202-1–245202-7.
29. Wagberg, T.; Hania, P. R.; Robinson, N. D.; Shin, J. H.; Matyba, P.; Edman, L. On the Limited Operational Lifetime of Light-Emitting Electrochemical Cells. *Adv. Mater.* **2008**, *20*, 1744–1749.
30. Matyba, P.; Maturova, K.; Kemerink, M.; Robinson, N. D.; Edman, L. The Dynamic Organic p-n Junction. *Nat. Mater.* **2009**, *8*, 672–676.
31. Pingree, L. S. C.; Rodovsky, D. B.; Coffey, D. C.; Bartholomew, G. P.; Ginger, D. S. Scanning Kelvin Probe Imaging of the Potential Profiles in Fixed and Dynamic Planar LECs. *J. Am. Chem. Soc.* **2007**, *129*, 15903–15910.
32. Slinker, J. D.; DeFranco, J. A.; Jaquith, M. J.; Silveira, W. R.; Zhong, Y. W.; Moran-Mirabal, J. M.; Craighead, H. G.; Abruna, H. D.; Marohn, J. A.; Malliaras, G. G. Direct Measurement of the Electric-Field Distribution in a Light-Emitting Electrochemical Cell. *Nat. Mater.* **2007**, *6*, 894–899.
33. Robinson, N. D.; Shin, J. H.; Berggren, M.; Edman, L. Doping Front Propagation in Light-Emitting Electrochemical Cells. *Phys. Rev. B* **2006**, *74*, 155210-1–155210-5.
34. Pei, Q. B.; Yang, Y.; Yu, G.; Zhang, C.; Heeger, A. J. Polymer Light-Emitting Electrochemical Cells: *In Situ* Formation of a Light-Emitting p-n Junction. *J. Am. Chem. Soc.* **1996**, *118*, 3922–3929.

35. Slinker, J. D.; Gorodetsky, A. A.; Lowry, M. S.; Wang, J. J.; Parker, S.; Rohl, R.; Bernhard, S.; Malliaras, G. G. Efficient Yellow Electroluminescence From a Single Layer of a Cyclometalated Iridium Complex. *J. Am. Chem. Soc.* **2004**, *126*, 2763–2767.
36. Muhlbacher, D.; Neugebauer, H.; Cravino, A.; Sariciftci, N. S.; Van Duren, J. K. J.; Dhanabalan, A.; Van Hal, P. A.; Janssen, R. A. J.; Hummelen, J. C. Comparison of Electrochemical and Spectroscopic Data of the Low-Bandgap Polymer PTPTB. *Mol. Cryst. Liq. Cryst.* **2002**, *385*, 205–212.
37. Lide, D. R. *CRC Handbook of Chemistry and Physics*, 83rd ed.; CRC Press: Boca Raton, FL, 2002−2003; pp 12−130.
38. Hoven, C. V.; Garcia, A.; Bazan, G. C.; Nguyen, T. Q. Recent Applications of Conjugated Polyelectrolytes in Optoelectronic Devices. *Adv. Mater.* **2008**, *20*, 3793–3810.
39. Becker, H.; Spreitzer, H.; Ibrom, K.; Kreuder, W. New Insights into the Microstructure of Gilch-Polymerized PPVs. *Macromolecules* **1999**, *32*, 4925–4932.
40. Charrier, D. S. H.; Kemerink, M.; Smalbrugge, B. E.; De Vries, T.; Janssen, R. A. J. Real *versus* Measured Surface Potentials in Scanning Kelvin Probe Microscopy. *ACS Nano* **2008**, *2*, 622–626.